



Adaptive frequency decomposition of EEG with subsequent expert system analysis

C.S. Herrmann^{a,*}, T. Arnold^a, A. Visbeck^b, H.-P. Hundemer^c, H. C. Hopf^b

^aMax Planck Institute of Cognitive Neuroscience, PO Box 500 355, D-04303 Leipzig, Germany

^bDepartment of Neurology, University of Mainz, Langenbeckstr. 1, D-55131 Mainz, Germany

^cLilly Germany, Saalburgstr. 153, D-61350 Bad Homburg, Germany

Received 30 November 2000; accepted 6 March 2001

Abstract

We present a hybrid system for automatic analysis of clinical routine EEG, comprising a spectral analysis and an expert system. EEG raw data are transformed into the time–frequency domain by the so-called adaptive frequency decomposition. The resulting frequency components are converted into pseudo-linguistic facts via fuzzification. Finally, an expert system applies symbolic rules formulated by the neurologist to evaluate the extracted EEG features. The system detects artefacts, describes alpha rhythm by frequency, amplitude, and stability and after artefact rejection detects pathologic slow activity. All results are displayed as linguistic terms, numerical values and maps of temporal extent, giving an overview about the clinical routine EEG. © 2001 Elsevier Science Ltd. All rights reserved.

Keywords: EEG; Spectral analysis; Expert system; Fuzzy logic

1. Introduction

Visual analysis and diagnosis of EEGs is a very time-consuming and tedious task. Numerous approaches have been made to automatically extract the main characteristics of an EEG. To name a few of them, Hjorth [1] calculated signal theoretical parameters of EEG waves, Dumermuth [2] applied the Fast Fourier Transform, Arle and Simon [3] determined the fractal dimension, Witte et al. [4] applied the Hilbert transform, Krajča et al. [5] used adaptive segmentation, Nakamura et al. [6] developed statistical measures and Schiff et al. [7] applied a wavelet transform. All of the above methods operate on a mathematical basis and basically transform the EEG data into a new numerical representation.

* Corresponding author. Tel.: +49-341-9940-250; fax: +49-341-9940-204.

E-mail address: herrmann@cns.mpg.de (C.S. Herrmann).

In contrast to the above-mentioned methods, our approach, which also generates new parameters, additionally interprets these parameters by means of Artificial Intelligence. Our hybrid system combines a new method of analysing EEGs in the time–frequency domain with a subsequent evaluation of the parameters by a neurological expert system using Fuzzy Logic.

The most common pre-processing of EEGs is the frequency representation via a Fourier transform. The restricted frequency resolution of this method can be a drawback which we wanted to overcome by an alternative approach. The numerical features are extracted from EEG raw data utilizing a special kind of spectral decomposition—the adaptive frequency decomposition—and are then transformed into pseudo-linguistic facts by means of Fuzzy Logic [8]. Thereafter, these facts are checked by the rules of an expert system [9] for classifying and excluding artefactual time intervals from further evaluation. As a next evaluation step, based upon statistical parameters, the alpha activity is described separately for each channel. Finally, focal or generalized slowing is detected according to the rules formulated by the physician.

Mapping the power of predefined frequency bands as scalp topographies as well as mapping of frequencies of short time intervals has been used widely for the analysis of EEG [10–12] and was found particularly useful for the detection of focal lesions [13, p. 1090]. We wanted to go one step further by computing maps of the temporal extent of important frequency bands relative to the total evaluated registration time. In contrast to other mapping techniques, where the *amplitude* of selected time intervals is mapped across the scalp, our approach displays the temporal extent of only those frequency components which have been detected throughout the whole EEG. This measure seems to be more reliable than just the amplitude and it can be computed for the whole EEG without selecting certain time periods, since artefacts are automatically excluded by the rule-based analysis.

2. Methods

Subjects: We analysed 20 EEGs selected arbitrarily from clinical routine EEG recordings. Patients aged from 18 to 88 years underwent EEG examinations for different neurological diseases. Their overall diagnoses together with the classifications of their EEGs are shown in Table 1. One neurologist arrived at these diagnoses without knowledge of the automatic results of the described system. All selected EEGs contained artefacts.

Data acquisition: The EEGs were acquired on a MicroMed BrainQuick2 system with a 0.32 Hz highpass ($T = 0.5$ s), a 1500 Hz anti-aliasing lowpass filter (40 dB/octave) and a hardware sampling rate of 4096 Hz. For digital storage, the raw data were down-sampled at 256 Hz with an anti-aliasing lowpass filter of 120 Hz (40 dB/octave). The amplitude range of ± 400 μ V was digitized into 12 bits resulting in an A/D precision of 195 nV/bit. There was no further digital notch, low- or highpass filtering applied to the data.

Each EEG included the signals of all electrodes of the international 10–20-system [14] measured against an additional reference electrode placed near the Cz electrode, i.e. a monopolar montage as described by Reilly [15]. As our method is based on the average montage of an EEG, the original signals were re-referenced against the numerical average (Avg) of all 10–20-electrodes excluding Fp1 and Fp2 (additional electrodes A1 and A2 were also excluded). We choose a reference montage because it provides a topologically unbiased representation of the EEG potentials, whereas bipolar montages can suffer from substantial distortions [16].

Table 1
Overall diagnosis and classification of the EEG for 20 selected patients

ID	Diagnosis	Classification		
		Normal	Abnormal	Pathologic
01	Headache	×		
02	Epilepsy	×		
03	Glioblastoma			Focal slow delta activity
04	Cerebral ischemia			Generalized slow delta/theta activity
05	Astrocytoma			Focal slow delta/theta activity
06	Multiple sclerosis			Focal slow theta activity
07	Cerebral ischemia		Slow alpha variant	
08	Wernicke's encephalopathy	×		
09	Chronique fatigue syndrom	×		
10	Synkope	×		
11	Epilepsy	×		
12	Headache	×		
13	Epilepsy			Focal slow delta activity
14	Headache	×		
15	Cerebral ischemia	×		
16	Cerebral hemorrhage			Generalized flow delta/theta activity
17	Multiple sclerosis	×		
18	Commotio cerebri	×		
19	Cerebral ischemia	×		
20	Epilepsy			Focal slow delta/theta activity

Sketch of method: Our method is comprised of two major parts, namely the adaptive frequency decomposition and the expert system analysis, as shown in Fig. 1. The adaptive frequency decomposition transforms the raw data of each channel into the time–frequency domain by spectral analysis. In a second step, the resulting spectral data are analysed in the time–frequency domain to extract the dominant frequency components over time for each channel. During the subsequent expert system analysis, the extracted components of all channels are converted into a linguistic representation by means of fuzzification. Afterwards an expert system applies rules, formulated by a neurological expert, to these linguistic facts in order to infer the evidences finally reported to the user.

2.1. Spectral analysis

2.1.1. Segmentation of data

The spectral analysis consists of a sequence of spectral transformations of the raw data at short intervals. Each individual transformation computes the power spectral density (PSD) called the

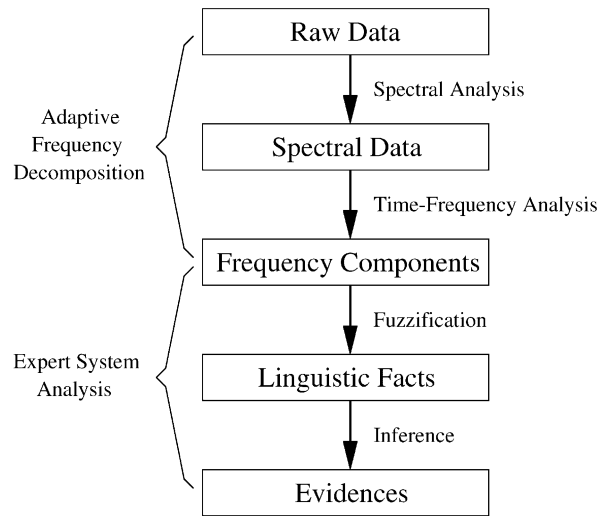


Fig. 1. Schematic depiction of method.

spectrum of an interval of length T , where each interval has the offset $T/2$ relative to the preceding one. The overlap of the intervals prevents to some degree the splitting of EEG phenomena across several intervals. The n th interval is defined as

$$I_n = [n(T/2), n(T/2) + T] \quad (n \geq 0).$$

The choice of the interval length T has an impact on the accuracy of the method because each transformation reflects the sum of all activity during the transformed interval. If T is large, short EEG phenomena and phenomena with a low amplitude may be suppressed by other activity during the same interval. On the other hand, if T is small, long phenomena are split across several intervals. We tested various values between $T = 0.5$ and 2 s with several EEGs. Taking into account that we want to detect graphoelements with durations of approximately 1 s or less (e.g. fast and slow waves as well as artefacts), we choose $T = 1$ s, which gave the best results in combination with the following steps of the analysis.

2.1.2. Spectral transformation

A common algorithm to compute the PSD of a discrete time series is the Fast Fourier Transform (FFT) [17] which has been applied to EEG analysis in the past [2,18,19]. One inherent drawback of the FFT is its discrete frequency resolution of $\Delta F = 1/T$. In case of an interval length of $T = 1$ s this leads to a resolution of $\Delta F = 1$ Hz, which is too coarse for medical diagnosis. To extract the dominant frequency components and their evolution over time, a frequency resolution that is at least 10 times more precise is needed. One solution to this problem could be the combination of the FFT with extensive zero-padding and an appropriate data windowing technique like Bartlett or Welch windows.

We decided to use a different approach that computes the PSD based on the so-called autoregressive model (AR) [20]. The advantage of an AR model is that it provides a continuous estimator of

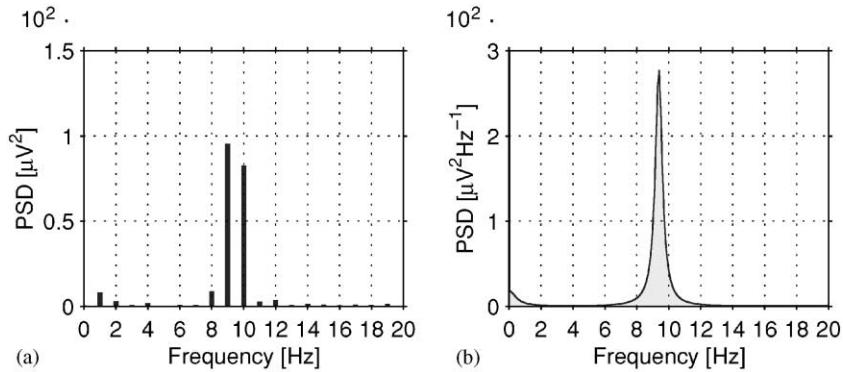


Fig. 2. (a) FFT spectrum and (b) AR spectrum of 1 s of sample data.

the PSD which can be evaluated at any desired resolution without additional preprocessing steps. We chose a model order of $M = 10$ which Praetorius et al. [21] stated as being sufficient to capture all essential features of an EEG frequency spectrum. Fig. 2 shows the FFT and the AR spectrum of 1 s of sample data. On the left side is the result of a standard FFT and on the right side is the result of the AR model adapted from Press et al. [22, pp. 564–575] with a resolution of $\Delta F = 0.1$ Hz.

Every line in the FFT spectrum represents the power of a frequency interval with a width of 1 Hz symmetric around this line. In contrast to this, the power $P(f_a, f_b)$ of a frequency interval $[f_a, f_b]$ is computed in the AR spectrum by integrating the power spectral density $\text{PSD}(f)$ according to

$$P(f_a, f_b) = \int_{f_a}^{f_b} \text{PSD}(f) df.$$

Both methods yield similar results concerning the absolute power of the signal, but the AR spectrum allows a more precise extraction of the underlying frequency in the data compared to the standard FFT.

2.1.3. Computational costs

Although we did no direct comparison of the computational costs when using FFT spectra rather than AR spectra, some general statements can be made. The computation time of an FFT spectrum is in the order of $O(N \log N)$ compared to $O(MN)$ for an AR model, with N being the number of samples. In addition, each AR spectrum requires constant computation time for the evaluation of the AR model with the desired frequency resolution. However, to achieve a frequency resolution of $\Delta f = 0.1$ Hz with zero-padding FFT, 9 s of additional zeros would have to be transformed for every second of data. Aside from these theoretical thoughts, our approach performs sufficiently for our experimental interests in practice. The computation of the AR spectra for all 19 channels of an EEG recording of half an hour takes about 7 min on a Linux-PC with an AMD K6-II 300 MHz CPU and 64 MB of RAM. This indicates that all channels of the 10–20-system can be transformed into the time–frequency domain in real time without additional DSP hardware, i.e. could be done on-line.

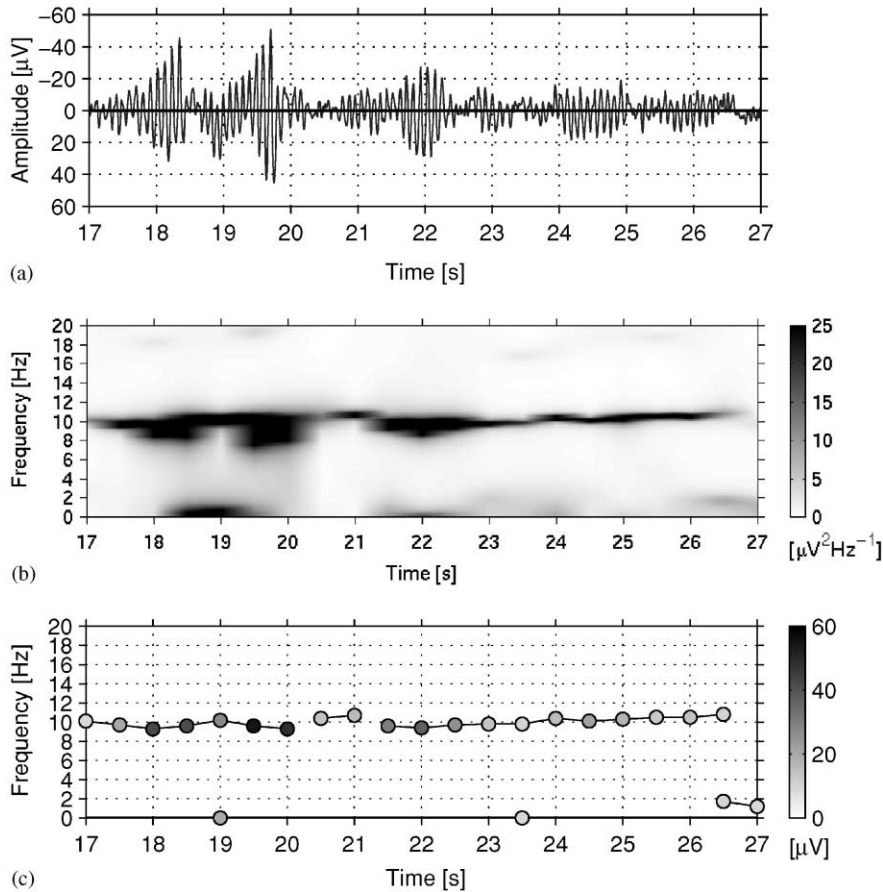


Fig. 3. Adaptive frequency decomposition transforms 10 s of raw data (a) into spectral data (b) and extracts frequency components (c) that are connected to chains.

2.2. Time–frequency analysis

2.2.1. Extraction of components

The time–frequency domain of a channel is built from the sequence of AR spectra. Fig. 3b shows the spectral data resulting from the transformation of 10 s of raw data presented in Fig. 3a, with the amplitudes of the spectra coded as grayscales. For a better visualization, the amplitudes are cropped at $25 \mu\text{V}^2 \text{Hz}^{-1}$ which turns the peaks in the spectra more or less to plateaus. The alpha activity in the sample data is represented as a narrow band at about 10 Hz. The extraction of such connected frequency components that dominate the EEG over a certain period of time is the main task of the adaptive frequency decomposition that will be described below.

In a first step, the spectrum of each interval I_n is decomposed into separate frequency components. We define a frequency component C_i as a triplet consisting of a time stamp t_i , a frequency f_i and the power P_i associated with that frequency:

$$C_i = (t_i, f_i, P_i).$$

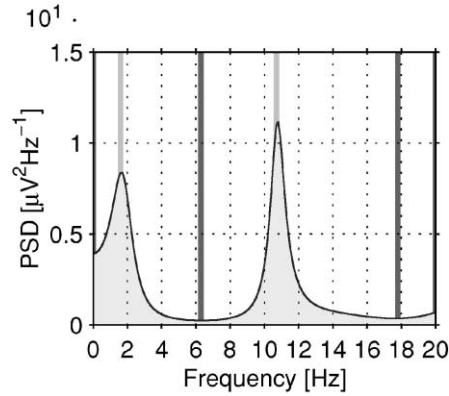


Fig. 4. Frequency components of 1 s of sample data.

The time stamp of a component is set to the centre of the corresponding interval I_n , i.e.

$$t_i = nT + \frac{T}{2}.$$

For the purpose of extracting the other information, the spectrum is segmented into frequency intervals defined either by the frequencies of its local minima or by the borders of the spectrum. If a frequency interval contains a local maximum, the power of this frequency interval is computed by numerical integration of the PSD and associated with the frequency of the local maximum. We also consider local maxima at the 0 Hz borders of the spectra, because certain rhythmic activity in the EEG, such as irregular delta activity, have so-called $1/f$ spectra. Otherwise, no frequency components would be extracted from this type of spectra.

Fig. 4 shows a spectrum derived from 1 s of the sample data shown in Fig. 3a with vertical lines marking the frequencies of the local maxima and the boundaries of the frequency intervals. The spectral data represent the vanishing alpha activity at 26.5 s followed by a slow shift of the signal back to the baseline. In this case the above-described algorithm extracts the following frequency components:

$$C_1 = (26.5 \text{ s}, 1.7 \text{ Hz}, P(0.0 \text{ Hz}, 6.3 \text{ Hz})),$$

$$C_2 = (26.5 \text{ s}, 10.8 \text{ Hz}, P(6.3 \text{ Hz}, 17.8 \text{ Hz})).$$

One goal of the adaptive frequency decomposition is to focus on salient information about the EEG, so that only dominant frequency components should be extracted from the spectra. This is achieved by selecting only those components with a power larger than ε times the total power of all components in that spectrum. A component C_i out of n components C_1 to C_n of a single spectrum is therefore chosen if

$$P_i > \varepsilon \sum_{j=1}^n P_j.$$

We choose $\varepsilon = 0.33$, i.e. a valid component must occupy at least 33% of the total power of all components. As a desired consequence, in practice there is usually a maximum of two frequency

components at the same time. Limiting the minimum power of a component also makes the decomposition robust against any noise in the spectrum which may arise from noisy raw data.

2.2.2. Composition of chains

After decomposition of all spectra, a set of separate frequency components is gained but no information about the evolution of frequency components over time is revealed. Therefore, in a second step, the time–frequency analysis searches components that can be connected to chains. Two components C_i and C_j can be connected if they are directly consecutive and their frequencies do not differ for more than a threshold δ . Thus, the following requirements have to be met:

$$|t_i - t_j| = T/2, \quad |f_i - f_j| \leq \delta.$$

We choose $\delta = 1$ Hz, which gives reasonable results compared with visual classifications.

Fig. 3c shows the extracted frequency components from the sample data as grayscaled dots where the chains are represented by the connecting lines between the components. Because the power of a frequency component C_i is a rather abstract quantity, it is re-transformed into an amplitude a_i expressed in μV for easier interpretation. This value is the peak-to-peak amplitude of a sinusoidal signal with the power P_i in the order of

$$a_i = \sqrt{8P_i}.$$

This leads to new components where the spectral power is replaced by the amplitude:

$$C_i = (t_i, f_i, a_i).$$

One has to keep in mind that these artificial amplitudes only express the mean amplitude of a component during an interval with length T and not the maximum peak-to-peak amplitude.

2.2.3. Statistical measures

With each single component having a frequency f_i and an amplitude a_i it is straightforward to define related statistical measures for a set of components. A set may consist of the frequency components of a single chain or all frequency components in a neurological frequency band. For any such set $S = \{C_1, \dots, C_n\}$, we define the weighted mean amplitude \bar{a} , the weighted mean frequency \bar{f} and the weighted standard deviation d of frequency as follows:

$$\bar{a} = \frac{\sum_{i=1}^n w_i a_i}{\sum_{i=1}^n w_i},$$

$$\bar{f} = \frac{\sum_{i=1}^n w_i f_i}{\sum_{i=1}^n w_i},$$

$$d = \sqrt{\frac{\sum_{i=1}^n w_i (f_i - \bar{f})^2}{\sum_{i=1}^n w_i}}.$$

We assign the amplitude of each component to the weight, i.e. $w_i = a_i$, with the intention that high-amplitude components should have a greater effect on the measures. It follows that

high-amplitude deviants from the weighted mean frequency lead to higher values of the standard deviation than low-amplitude deviants.

If a set S is chosen from the frequency components in a continuous time interval of duration D , it is easy to compute the fraction of time during which the corresponding activity is present. We call this the temporal extent e of the activity. With $|S|$ denoting the number of components in the set, we define

$$e = \frac{|S|T/2}{D}.$$

It is obvious that the above definition is only valid if S contains no frequency components with identical time stamps. It should also be stated that all of the introduced statistical measures are independent of any connections between the frequency components.

2.3. Fuzzification

Niedermeyer and Lopes da Silva wrote: “Electroencephalographers may indicate in their reports a certain amplitude range, such as ‘alpha rhythm from 20–30 μV ’ or, even better, limit themselves to statements such as ‘of medium voltage’ or ‘of low to medium voltage’”. [23, p. 12]. Taking up this explicit request for a rather linguistic than numeric description of the EEG, our expert system analysis is based on pseudo-verbal attributes close to the terminology of the neurologist [24]. Hence, to make the numerical measures accessible to the symbolic rules in the expert system their values have to be fuzzified.

2.3.1. Membership functions

The transformation from numerical values to linguistic terms requires the definition of appropriate membership functions for each term [25]. A set of membership functions forms the so-called linguistic variable of the measure. Such a linguistic variable should first and foremost reflect the terminology that the expert, in our case the neurologist, uses when classifying the measure. Different authors have proposed different classifications for the frequency of EEG activity and the amplitude of the alpha rhythm [26]. We tried to extract the common features of these classifications, which led us to the linguistic variables presented in Fig. 5 describing the measures frequency (a), amplitude (b), standard deviation of frequency (c) and temporal extent (d) of EEG activity. The displayed functions map the numerical values of the measure to degrees of membership μ of the according term with 0 indicating no membership and 1 indicating total membership.

A frequency component, like e.g. $C = (26.5 \text{ s}, 10.8 \text{ Hz}, 17.5 \mu\text{V})$, is therefore fuzzified by the expert system as activity with an alpha frequency (certainty of 100%) and low amplitude (certainty of 75%) to medium amplitude (certainty of 25%).

2.4. Inference

After fuzzification, the frequency components are accessible to the expert system as the so-called linguistic facts. The symbolic rules were formulated by a neurologist and describe the detection of EEG phenomena in an intuitive IF–THEN style. They are clustered into modules and applied to the facts in several stages to infer the final evidences reported by the system (cf. Fig. 6).

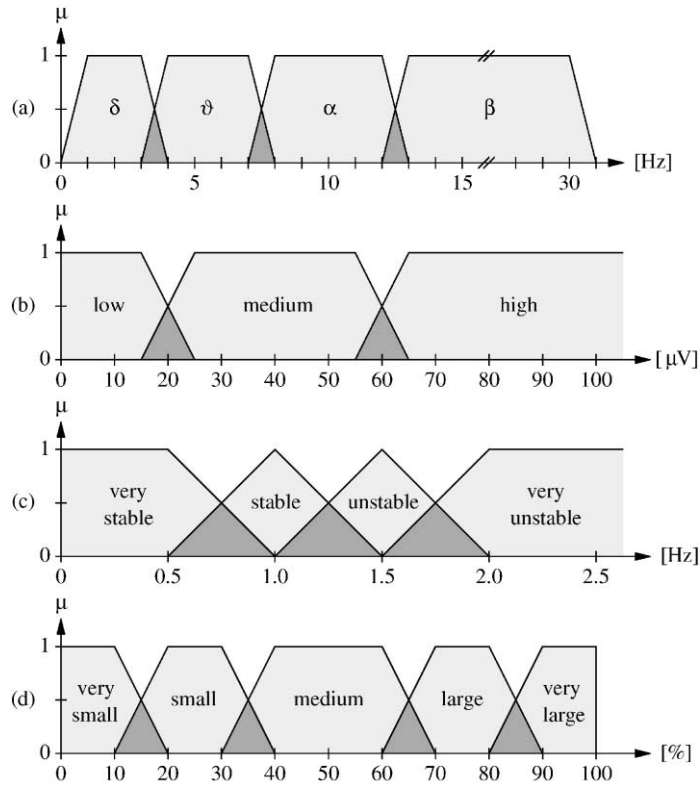


Fig. 5. Membership functions for the linguistic variables of frequency (a), amplitude of alpha rhythm (b), standard deviation of frequency (c) and temporal extent (d) of EEG activity.

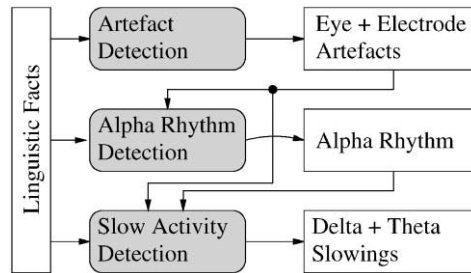


Fig. 6. Processing stages of expert system analysis. The successive application of rules for detecting artefacts, the alpha rhythm and slow activity to the linguistic facts leads to the inferred evidences.

The first stage of the expert system detects eye movements and electrode artefacts. This information is important for the following stages of the analysis, because their results could be biased when not taking into account artefactual intervals. The second stage tries to determine the alpha rhythm within the EEG from the frequency information represented by the linguistic facts. As described below, this information is also necessary for the module that deals with the detection of slow activity, which is

(currently) the last stage of the analysis. We are using the public-domain software FuzzyCLIPS [27], that was derived from NASA's expert system CLIPS [28] to implement our rules. In the following, we will describe the three modules of the expert system.

2.4.1. Artefact detection

Due to the well-understood origin of eye-movement artefacts, their detection is mainly based on the topographic distribution of synchronous slow activity. Eye movements are usually characterized by neurologists as high-amplitude activity in the delta or theta frequency band, which have a symmetric, bilateral maximum in the fronto-polar electrodes (Fp1, Fp2) for vertical eye movements and in frontal electrodes (F3, F4) for horizontal eye movements. As described in [29], we implemented a set of rules that searches the complete EEG for synchronous activity that matches the description given above. To be classified as eye-movement artefact there also has to be a monotonous decrease in the amplitude of any slow activity extracted from the adjacent electrodes. The corresponding interval is then marked as eye-movement artefact.

Electrode artefacts can be characterized as high-amplitude activity in one or more electrodes with directly adjacent electrodes showing no or only low-amplitude activity in the same frequency range at the same time. Additional rules scan the EEG for time intervals that match this description and mark them as electrode artefacts. These intervals are excluded from any further analysis by the expert system.

2.4.2. Alpha rhythm detection

The purpose of this module is the detection of a clear-cut alpha rhythm within the EEG at rest with closed eyes. But during routine EEG recordings certain reactions to external stimulation are tested, namely opening the eyes (Berger effect), hyperventilation and photic driving. Markers indicating the beginning and the end of these epochs are placed in the EEG by the technician. Hence, these epochs can easily be excluded from the analysis performed in this stage. Intervals that are marked during the first stage to contain eye-movement artefacts are not excluded, as these artefacts do not interfere with the analysis of alpha frequency.

From the remaining sections of the EEG, the statistical measures described in Section 2.2, i.e. mean amplitude, mean frequency, the standard deviation and the temporal extent of activity in the alpha frequency band, are computed for each electrode. Afterwards, the posterior electrodes are investigated for stable or very stable alpha activity with at least medium temporal extent. Of all electrodes which fulfill these criteria the electrode showing the highest mean amplitude is considered to best represent the alpha rhythm.

As additional information for the neurologist, the same procedure is carried out for the interval during which the patient had open eyes. Two maps of the temporal extent of alpha activity are then generated which allow a direct comparison of the stimulation interval with the rest of the EEG.

For statistical comparison of visual and automatic alpha analysis, the correlation coefficient (CI) was calculated for the computed parameters temporal extent, mean frequency and mean amplitude of the alpha rhythm. While the frequencies could be correlated directly the linguistic attributes had to be assigned numerical values at first. The levels *very small*, *small*, *medium*, *large* and *very large* of the attribute temporal extent (cf. Fig. 5d) were assigned numbers from 1 to 5, respectively. The levels *low*, *medium* and *high* of the attribute amplitude were assigned the values 1, 2 and 3, respectively.

2.4.3. Slow activity detection

The presence or absence of slow activity and its distribution is a main criterion in EEG interpretation. Therefore, the third module computes the same statistical measures as used in the previous stage, but this time for the delta and theta frequency band. In addition to any stimulation intervals, artefactual sections resulting from eye movements are excluded. This non-pathologic activity would otherwise interfere with the examined frequency bands and bias the results.

A problem arises when activity in the delta and theta frequency band are automatically processed in this way. Numerous slow potentials of negligible amplitude contaminate the digital EEG which are usually disregarded by the human inspector. In order to simulate the selective focusing on slow waves with amplitudes differing considerably from background activity, we oriented the computation to the alpha rhythm [30]. Hence, slow activity with amplitudes smaller than the mean amplitude of the previously detected alpha rhythm is discarded.¹ This procedure is to be preferred over an absolute threshold, since it adapts to the overall characteristics of the individual EEG. If no alpha rhythm was detected this part of the analysis is skipped and a warning is generated to indicate that no alpha rhythm was found. Electrodes that were found to have a temporal extent of delta or theta activity which is at least small are reported in the evidences.

Again, this procedure is carried out for the stimulation interval as well, in this case hyperventilation, to allow a direct comparison to the rest of the EEG.

3. Results

3.1. Artefacts

Fig. 7 shows the stepwise elimination of delta activity (a) which is contained in the frequency spectrum of a healthy subject. In a first step, all slow activity with amplitudes lower than the mean alpha rhythm is disregarded (b). Still, there is a substantial amount of delta activity (close to 20%) resulting from eye-movement artefacts which would be impossible to differentiate from pathological frontal slow potentials. In a further step of applying the rules for the detection of eye movements, this slow activity is also discarded. This leads to the map shown in Fig. 7c where the remaining delta activity has a temporal extent of less than 5% of the recording time. If slow activity is still present in the artefact-free map, all electrodes with a temporal extent of at least small ($\geq 10\%$) are listed in Table 4.

The rule-based approach of analysing various artefacts by means of pseudo-verbal rules from a neurologist in an expert system reached a high degree of correctness in classifying artefacts. We detected eye-movement artefacts in the delta range and blink artefacts in the theta range due to their bilateral occurrence in frontal electrodes with a frontopolar maximum that decreases briskly towards more posterior electrodes. The eye-movement artefact detection yields a discrimination index P_r ($P_r = \text{hitrate} - \text{false alarms}$)² of 87.8% [29]. The performance of the system can still be increased by fine-tuning the thresholds for the minimum amplitude of artefacts, avoiding false positive classifications for very low amplitude eye movements.

¹ The mean amplitude of the alpha activity is usually much lower than the visible peaks of alpha activity.

² This measure was introduced by Snodgrass and Corwin [31].

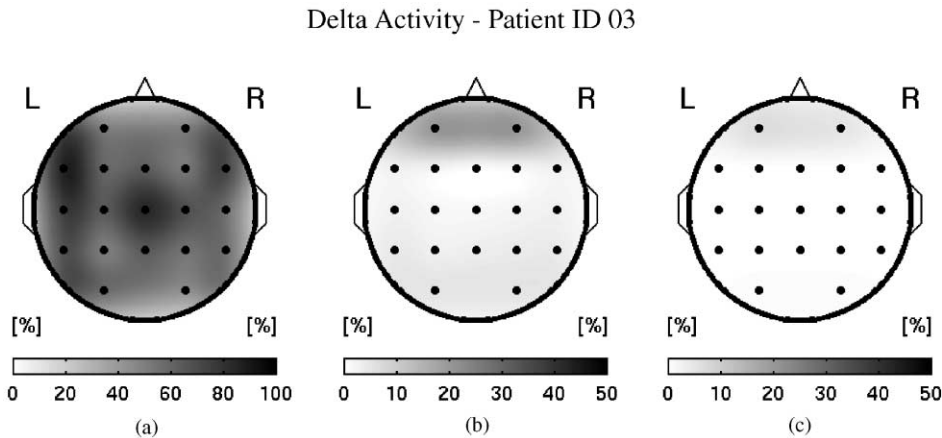


Fig. 7. Temporal extent of delta activity with regard to total recording length before (a) and after (b) thresholding with the mean amplitude of previously detected alpha rhythm. Application of the rules for eye-movement artefacts leads to the desired physiologic map without delta activity (c) of a healthy subject. Note the different scale for (a).

We also detect electrode artefacts when single electrodes show high amplitudes while adjacent electrodes show no correlated amplitude increase. EMG artefacts are represented in the high-frequency bands which are disregarded in slow potential analysis due to the frequency selectivity. Very slow frequency artefacts from sweating or impedance variation are up to now also disregarded. Exclusion of artefactual time intervals avoids capturing eye-movement artefacts in maps of slow potentials (cf. Fig. 7).

3.2. Alpha rhythm

The alpha rhythm of all patients is shown in Table 2 for the expert's visual EEG interpretation (*visual*) and that of our system (*automatic*). Both data represent the temporal extent of the basic rhythm according to the linguistic variable (cf. Fig. 5d), its frequency with deviation, and amplitude.

Due to the use of linguistic variables, our system performs an automatic analysis which is based on the same verbal attributes as the physician's diagnosis. This makes the visual and automatic analysis comparable. In all 20 analysed EEGs, the automatic analysis of the alpha rhythm correlated strictly with the visual diagnosis (cf. Table 3).

After artefact elimination, the maps show the temporal extent of certain frequency bands. We picked out four representative maps for illustration shown in Fig. 8. The map for patient 3 was classified as an occipitally dominant alpha rhythm with large temporal extent. A more parieto-occipital topography was computed for patient 9.

3.3. Delta and theta slow activity

Fig. 9 shows the maps of the temporal extent of delta and theta activity for two patients. The upper left map demonstrates the large temporal extent (almost 50% of the time) of the delta activity in patient 3, who was visually diagnosed to have a strong, right-hemispheric delta focus. The theta

Table 2

Comparison of visual and automatic analysis concerning the alpha rhythm^a

ID	Visual			Automatic		
	Extent	Frequency (Hz)	Amplitude	Extent	Frequency (Hz)	Amplitude
01	Large	9.5–10	High	Large	10.2 (very stable)	Medium
02	Large	8	Medium	Very large	8.3 (very stable)	Medium
03	Very large	9.5	High	Very large	9.5 (very stable)	Medium
04	—	—	—	—	—	—
05	Large	10–11	Medium	Medium	9.3 (stable)	Medium
06	Very large	9.5	High	Very large	9.8 (very stable)	Medium
07	—	—	—	—	—	—
08	Medium	10	Medium	Medium	10.2 (stable)	Low
09	Large	9	Medium	Medium	8.3 (stable)	Low
10	Medium	9	Low	Medium	9.3 (stable)	Low
11	Medium	9	Medium	Medium	9.1 (stable)	Medium
12	Very large	9	High	Very large	8.9 (very stable)	Medium
13	Large	11.5	Medium	Large	10.9 (very stable)	Medium
14	Very large	10–11	Medium	Very large	9.9 (very stable)	Low
15	Large	10	Medium	Medium	10.2 (stable)	Medium
16	Medium	9–10	Medium	Large	9.2 (stable)	Low
17	Very large	9–10	High	Very large	9.4 (very stable)	Medium
18	Medium	10–11	Low	—	—	—
19	Large	9	High	Large	9.3 (very stable)	Medium
20	Large	7–8	Medium	Large	8.2 (stable)	Medium

^aFor patients 04 and 07 no alpha rhythm was visually classified. For patients 04, 07 and 18 no alpha rhythm was automatically detected.

Table 3

Correlation of the automatically calculated temporal extent, mean frequency and mean amplitude of the alpha rhythm with the visual diagnosis

Attribute	Correlation index	Significance level
Temporal extent	0.87	$p < 0.01$
Frequency	0.75	$p < 0.01$
Amplitude	0.83	$p < 0.01$

map on the right shows almost no sign of abnormal slow activity. In the lower two pictures, the maps for patient 16 show the diagnosed generalized bilateral cerebral disorder in the delta band (left) and even stronger in the theta band (right). These maps demonstrate how the system can differentiate between focal slowing (top) and diffuse slowings (bottom).

Table 4 shows the close correlation of the visual and the automatic analysis. The difference between focal (e.g. patient 3) and generalized (e.g. patient 11) slow activity is reflected in the number of detected electrodes. It was not possible to calculate a correlation coefficient, since the measures are not numerical. Nevertheless, we can compare the visual and automatic analysis. Among the EEGs which were visually classified to contain no slow activity (patients 1, 2, 8–12, 14, 15, 17–19) the maps show no signs of slow potentials except for two false positive classifications (patients 9

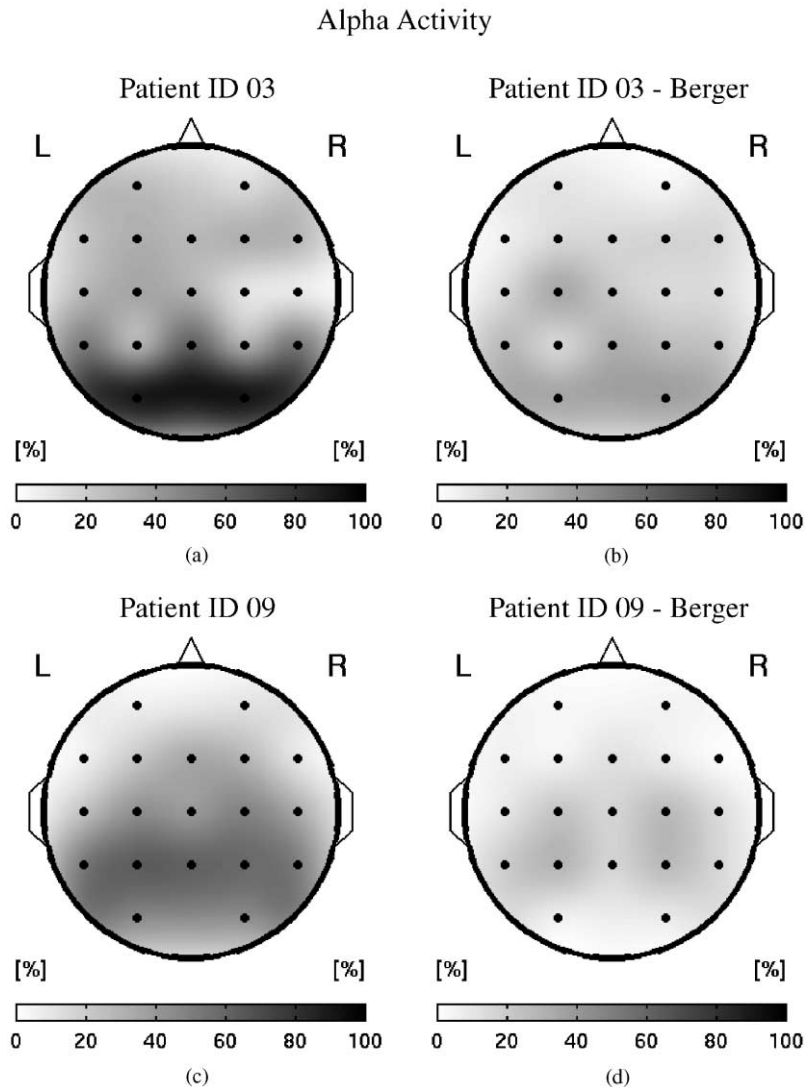


Fig. 8. Temporal extent of alpha activity for patient 03 (a) with regard to total recording length excluding reactivity testing and during Berger reactivity testing (b) and the same maps for patient 09 (c and d).

and 11) where the automatic analysis detected theta activity with small temporal extent (approx. 20%). In patient 11, these findings were due to unusually asymmetric eye artefacts which were not detected. In patient 9, the visual analysis of T5 and O1 was difficult due to strong artefactual contamination. This might be the reason why the automatically detected slight slowing of around 7 Hz in these electrodes was not detected by visual analysis. Retrospective visual analysis revealed that these slow potentials were actually present.

Also, for all EEGs containing slow potentials according to visual analysis (patients 3–7, 13, 16 and 20) the maps of delta and theta activity correlate closely with the visual diagnosis in showing

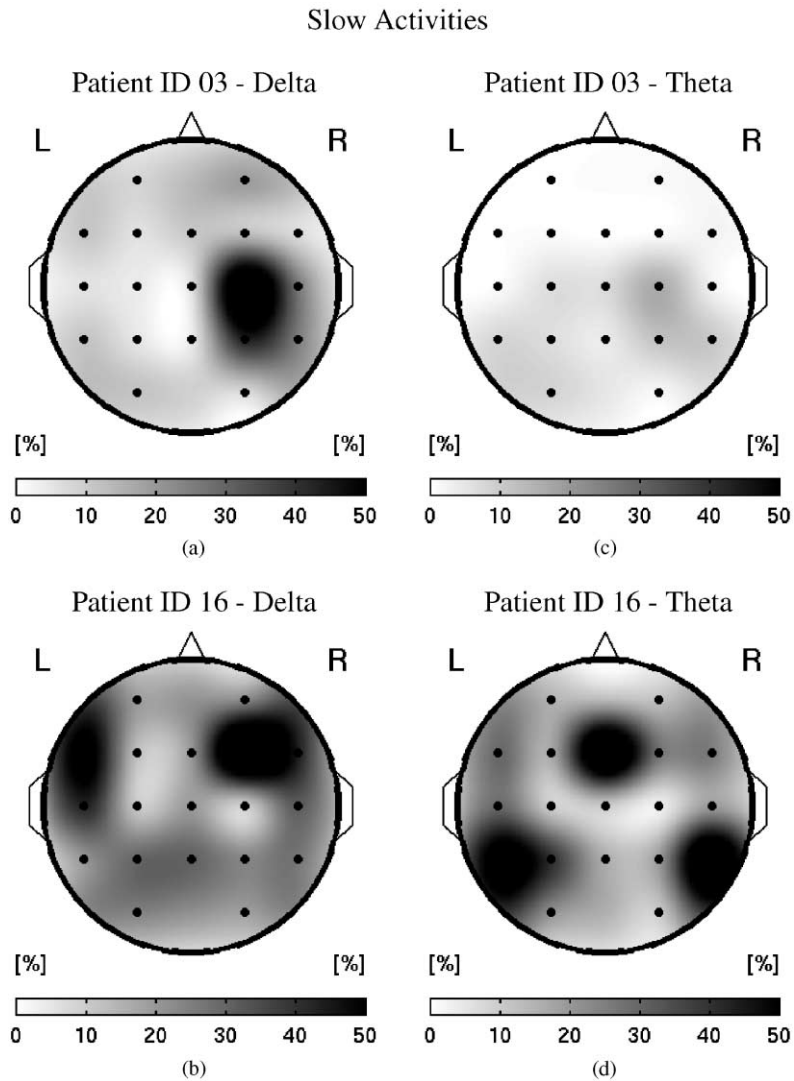


Fig. 9. Temporal extent of delta (left) and theta (right) activity for patient 03 (top) and patient 16 (bottom) with regard to total recording length excluding reactivity testing.

delta and theta activity with temporal extents between approximately 40% and 90% except for one false negative: Patient 6 was misclassified by our system as having no slow potentials with substantial temporal extent. Nevertheless, visual analysis yielded four time periods of 0.5–1 s duration with theta waves.

These epoches were too rare events for our system to be analysed in the statistical maps.³ Hence, the automatic system yielded 5% false negative (patient 6) and 10% false positive (patients 9 and 11) classifications.

³ In a refinement of our system we plan to evaluate each 1 s epoch separately to account for this type of phenomenon.

Table 4

Comparison of the automatically detected slow activity with the visual diagnosis^a

ID	Visual	Automatic	
		Delta	Theta
3	Localized slowing (delta), right centro-parietal/temporal, frontal	C4, P4, T4, T6	—
4	Generalized slowing (delta + theta)	!	!
5	Localized slowing (delta + theta), right temporal	T4, F8, T6	T6
6	Localized slowing (theta), left temporal	—	—
7	Generalized slowing (delta + theta), parieto-occipital	!	!
9	—	—	T5, O1
11	—	F8	—
13	Localized slowing (delta), left temporal	T3, F7, T5	—
16	Generalized slowing (delta + theta), alternating frontal, temporal	F4, F7, F8, T3, T4, Pz, P3, T6, O1, Fp2, P4, Cz, T5, Fz, O1	Fz, T6, T5, P3, T3, F7, F3, F8, O1
20	Localized slowing (delta + theta), right temporal	T4, F8, T6, T3	T4, F8, T6

^aThe ! indicates that in patients 4 and 7 the analysis could not be carried out, since no alpha rhythm was found, as described above. Note that only those patients are listed who were classified as having abnormal slow activity by either the visual or automatic analysis.

4. Discussion

The high correlation of our automatical analysis and the visual diagnosis suggests that the approach introduced here is a valuable tool for the neurologist that provides an overview of a whole routine EEG by summarizing a few intuitive (numerical and linguistic) parameters.

In order to automatically analyse an EEG in an expert system, it is necessary to transform the EEG into its frequency representation where the variables frequency and amplitude can be used to describe the EEG. This is mostly done by the FFT [2,18,19]. As described in Section 2.1, the FFT has the drawback of allowing only a limited frequency resolution unless numerical precision is enhanced with zero-padding. We wanted to overcome this drawback by using the AR method for estimating frequency spectra. Kay and Marple [32] showed that an AR model is a stable and accurate estimator of the PSD, if the transformed time series is the superposition of only a few sinusoidal generators. This condition is fulfilled by EEG data, because usually no more than two or three components explain about 90% of the variance in an EEG epoch. Therefore, we applied an autoregressive model to extract frequency components from EEG which has proved very efficient in EEG analysis [33–35]. We showed that this method provides frequency spectra which offer a better frequency resolution than the standard FFT without zero-padding.

For the purpose of analysing a whole routine EEG instead of just a short epoch, one needs to identify temporally extended frequency components. Our time–frequency analysis is able to track the

drifting frequency and alternating amplitudes of the frequency components over time. Since it does this individually for each patient, we call it *adaptive*.

One main aspect of our approach is to use the rule-based method of diagnosing data proposed by Artificial Intelligence. Other authors have also used approaches from Artificial Intelligence to analyse EEG in the past. Among them, Davey et al. [36] analysed steep potentials in an expert system for their epileptic nature and Dawant and Jansen [37] used two knowledge bases for pattern analysis and medical diagnosis. Jansen [38] compared a discriminant analysis [39], a syntactical analysis [40] and an Artificial Intelligence approach [41] and found the latter to have the best correlation with three independent neurologists. Our system fits into this framework of Artificial Intelligence approaches but uses a new preprocessing technique for transforming the raw EEG data into a symbolic representation—namely the adaptive frequency decomposition. In addition, the linguistic representation of rules as well as facts makes rule formulation and system supervision easy and intuitive. Diagnosis results can be traced back and the system can be refined to improve its behaviour.

A very promising approach to evaluate EEGs has also been to feed EEG data into neural networks (NNs) which are predetermined for mimetic analysis [18,42–45]. Si et al. [46] used a neural network (NN) to monitor pediatric EEG in intensive care units. They extract a number of statistical parameters, transform them into fuzzy logic to make them suitable for NN input and feed them into an NN which classifies the EEG. This approach is very similar to the one described by Herrmann [47]. Since one cannot predict the functional behaviour of an NN, we chose to use an expert system instead of an NN, in order to be able to exactly predict and retrospectively examine the inference mechanism which generates the diagnosis.

Numerous approaches have made use of mapping techniques to map amplitude or frequency of the EEG as scalp topographies (for an overview, see [11]). An inherent problem of all these methods is the necessary selection of artefact-free epochs from which to compute the maps. Otherwise, artefacts result in delta or theta peaks in the map—suggesting pathological slow activity, as we demonstrated in Fig. 7. Our approach uses neurological expert rules to eliminate artefacts prior to mapping. This would also be useful for the above mapping techniques, but we decided to map the temporal extent as a new measure for the functional significance of a frequency band. Since the map of the temporal extent of the alpha activity correlates very well with the visual diagnosis of the alpha rhythm ($CI=0.87$, $p < 0.01$), we take it to be a suitable measure to investigate the alpha rhythm. It should be taken into consideration in addition to the known mapping of amplitude and frequency. Also, the temporal extent of delta and theta activity correlates very well with the visual diagnosis. Hence, we propose this measure to be a good estimator for abnormal slow activity.

The very rarely occurring slow potentials present in one patient were not reported by the system, due to the short temporal extent. Nevertheless, all slow potentials are captured inside the system. In a future implementation we plan to evaluate each single slow potential with expert rules allowing a report of such rare activity.

In its current status, the system is not able to, and was not intended to, analyse epileptic discharges. But, due to its modular architecture, existing spike detection systems [48] can be used in addition to our pre-processing and can be fed into the expert system.

5. Summary

Visual analysis and diagnosis of EEGs is a very time-consuming and tedious task. Numerous approaches have been made to automatically extract the main characteristics of an EEG. To name a few of them, the calculation of slope parameters of EEG waves, the Fast Fourier Transform, the Hilbert transform and the wavelet transform have been applied to EEG signals. All of the above methods operate on a mathematical basis and basically transform the EEG data into a new numerical representation.

In contrast to the above-mentioned methods, our approach, which also generates new parameters, additionally interprets these parameters by means of Artificial Intelligence. Our hybrid system combines a new method of analysing EEGs in the time–frequency domain with a subsequent evaluation of the parameters by a neurological expert system using Fuzzy Logic.

The most common pre-processing of EEGs is the frequency representation via a Fourier transform. The restricted frequency resolution of this method can be a drawback which we wanted to overcome by an alternative approach. The numerical features are extracted from EEG raw data utilizing a special kind of spectral decomposition—the adaptive frequency decomposition—and are then transformed into pseudo-linguistic facts by means of Fuzzy Logic. Thereafter, these facts are examined by the rules of an expert system in order to classify and exclude artefactual time intervals from further evaluation. As a next evaluation step, based upon statistical parameters, the alpha activity is described separately for each channel. Finally, focal or generalized slowing is detected according to the rules formulated by the physician.

Mapping the power of predefined frequency bands as scalp topographies as well as mapping of frequencies of short time intervals has been used widely for the analysis of EEG and was found particularly useful for the detection of focal lesions. We wanted to go one step further by computing maps of the temporal extent of important frequency bands relative to the total evaluated registration time. In contrast to other mapping techniques, where the *amplitude* of selected time intervals is mapped across the scalp, our approach displays the temporal extent of only those frequency components which have been detected throughout the whole EEG. This measure seems to be more reliable than just the amplitude and it can be computed for the whole EEG without selecting certain time periods, since artefacts are automatically excluded by the rule-based analysis.

Acknowledgements

We would like to thank Bob Orchard at the National Research Council Canada for his excellent cooperation on the expert system software *FuzzyCLIPS*. In addition, we express our thanks to Jonathan Whitlock who improved the readability of this manuscript by polishing its English.

The research work for this project is funded by the German *Bundesministerium für Bildung und Forschung* (federal ministry of education and research) grant number 0311462.

References

- [1] B. Hjorth, EEG analysis based on time domain properties, *Electroencephalogr. Clin. Neurophysiol.* 29 (1970) 306–310.

- [2] G. Dumermuth, Fundamentals of spectral analysis in electroencephalography, in: A. Rémond, EEG Informatics. A Didactic Review of Methods and Applications of EEG Data Processing, Elsevier, Amsterdam, 1977, pp. 83–105.
- [3] J.E. Arle, R.H. Simon, An application of fractal dimension to the detection of transients in the electroencephalogram, *Electroencephalogr. Clin. Neurophysiol.* 75 (1990) 296–305.
- [4] H. Witte, M. Eiselt, I. Patakova, S. Petranek, G. Griessbach, V. Krajca, M. Rother, Use of discrete hilbert transformation for automatic spike mapping: a methodological investigation, *Med. Biol. Engng. Comp.* 29 (1991) 242–248.
- [5] V. Krajča, S. Petráněk, I. Patáková, A. Värri, Automatic identification of significant graphoelements in multichannel EEG recordings by adaptive segmentation and fuzzy clustering, *Int. J. Biomed. Comput.* 28 (1991) 71–89.
- [6] M. Nakamura, H. Shibasaki, K. Imajoh, S. Nishida, R. Neshige, A. Ikeda, Automatic EEG interpretation: a new computer-assisted system for the automatic integrative interpretation of aware background EEG, *Electroencephalogr. Clin. Neurophysiol.* 82 (1992) 423–431.
- [7] S.J. Schiff, A. Aldroubi, M. Unser, S. Sato, Fast wavelet transformation of EEG, *Electroencephalogr. Clin. Neurophysiol.* 91 (1994) 442–455.
- [8] L. Zadeh, Fuzzy sets, *Inf. Control* 8 (1965) 338–353.
- [9] B. Buchanan, E. Shortliffe, Rule-based Expert Systems, Addison-Wesley, Reading, MA, 1985.
- [10] D. Lehmann, Multichannel topography of human alpha EEG fields, *Electroencephalogr. Clin. Neurophysiol.* 31 (1971) 439–449.
- [11] F. Lopes da Silva, A critical review of clinical applications of topographic mapping of brain potentials, *Electroencephalogr. Clin. Neurophysiol.* 7 (1990) 535–551.
- [12] G. Pfurtscheller, F.H. Lopes da Silva, Functional Brain Imaging, Huber, Toronto, 1988.
- [13] E. Rodin, Clinical use of EEG topography, in: E. Niedermeyer, F. Lopes da Silva, *Electroencephalography, Basic Principles, Clinical Applications and Related Fields*, William & Wilkins, 1993.
- [14] M.R. Nuwer, G. Combi, R. Emerson, A. Fuglsang-Frederiksen, J.M. Guérit, H. Herrmann, A. Ikeda, F.J.C. Luccas, P. Rappelsburger, IFCN standards for digital recording of clinical EEG, *Electroencephalogr. Clin. Neurophysiol.* 106 (1998) 259–261.
- [15] E.L. Reilly, EEG recording and operation of the apparatus, in: E. Niedermeyer, F. Lopes da Silva, *Electroencephalography, Basic Principles, Clinical Applications and Related Fields*, William & Wilkins, 1993, pp. 104–124.
- [16] M.R. Nuwer, D. Lehmann, F. Lopes da Silva, S. Matsuoka, W. Sutherling, J.F. Vilbert, IFCN guidelines for topographic and frequency analysis of EEGs and EPs. Report of an IFCN committee, *Electroencephalogr. Clin. Neurophysiol.* 91 (1994) 1–5.
- [17] W. Cooley, J. Tukey, An algorithm for the machine calculation of complex Fourier series, *Math. Comput.* 19 (1965) 297–301.
- [18] G. Jandó, R. M. Siegel, Z. Horváth, G. Buzsáki, Pattern recognition of the electroencephalogram by artificial neural networks, *Electroencephalogr. Clin. Neurophysiol.* 86 (1993) 100–109.
- [19] B. Klöppel, Application of neural networks for EEG analysis, *Pharmacoelectroencephalography* 29 (1994) 39–46.
- [20] H. Wold, A Study in the Analysis of Stationary Time Series, Almquist & Wiksell, Stockholm, 1938.
- [21] H.M. Praetorius, G. Bodenstein, O.D. Creutzfeld, Adaptive segmentation of EEG records: a new approach to automatic EEG analysis, *Electroencephalogr. Clin. Neurophysiol.* 42 (1977) 84–94.
- [22] W. Press, S. Teukolsky, W. Vetterling, B. Flannery, Numerical Recipes in C: The Art of Scientific Computing, Cambridge University Press, Cambridge, 1992.
- [23] E. Niedermeyer, F. Lopes da Silva, *Electroencephalography, Basic Principles, Clinical Applications and Related Fields*, William & Wilkins, Philadelphia, 1993.
- [24] C.S. Herrmann, A hybrid fuzzy-neural expert system for diagnosis, in: C.S. Mellish (Ed.), *Proceedings of the 14th International Joint Conference on Artificial Intelligence (IJCAI)*, Morgan Kaufman, Los Altos, CA, 1995, pp. 494–500.
- [25] C.S. Herrmann, Symbolical reasoning about numerical data: a hybrid approach, *Appl. Intell.* 7 (1997) 339–354.
- [26] F. Lopes da Silva, Computer-assisted EEG diagnosis: pattern recognition and brain mapping, in: E. Niedermeyer, F. Lopes da Silva (Eds.), *Electroencephalography, Basic Principles, Clinical Applications and Related Fields*, William & Wilkins, Baltimore, 1993, pp. 1063–1086.
- [27] National Research Council Canada, FuzzyCLIPS User's Guide Version 6.02A, Knowledge Systems Laboratory, 1994.

- [28] NASA, CLIPS Reference Guide, Artificial Intelligence Section, 1993.
- [29] C.S. Herrmann, T. Arnold, A. Visbeck, H.P. Hundemer, H.C. Hopf, Rule-based artefact rejection for pre-processing event-related potentials, *Electroencephalogr. Clin. Neurophysiol.* 107 (1998) 52P.
- [30] Niebeling, Einführung in die Elektroenzephalographie, Springer, Berlin, 1980.
- [31] J.G. Snodgrass, J. Corwin, Pragmatics of measuring recognition memory: applications to dementia and amnesia, *J. Exp. Psychol.* 117 (1988) 34–50.
- [32] S. Kay, S. Marple, Spectrum analysis—a modern perspective, *Proc. IEEE* 69 (1981) 1380–1419.
- [33] L.H. Zetterberg, Means and methods for processing of physiological signals with emphasis on EEG analysis, in: J.e.a. Lawrence (Ed.), *Advances in Biology and Medical Physics*, Vol. 16, Academic Press, New York, 1977, pp. 41–91.
- [34] E.A. Stolz, Multivariate autoregressive models for classification of spontaneous electroencephalogram during mental tasks, Ph.D. Thesis, Department of EE, Colorado State University, 1995.
- [35] C.W. Anderson, E.A. Stolz, S. Shamsunder, Multivariate autoregressive models for classification of spontaneous electroencephalographic signals during mental tasks, *IEEE Trans. Biol. Engng.* 45 (1998) 277–286.
- [36] B.L.K. Davey, W.R. Fright, G.J. Carroll, R.D. Jones, Expert system approach to detection of epileptiform activity in the EEG, *Med. Biol. Engng. Comp.* 27 (1989) 365–370.
- [37] B.M. Dawant, B.H. Jansen, Coupling numerical and symbolic methods for signal interpretation, *IEEE Trans. Syst. Man Cybern.* 21 (1991) 115–124.
- [38] B.H. Jansen, Qualitative EEG analysis in renal disease, in: F.H. Lopes da Silva, W. Storm van Leeuwen, A. Rémond, *Clinical Applications of Computer Analysis of EEG and other Neurophysiological Signals (Handbook of Electroencephalography and Clinical Neurophysiology)*, Vol. 2, Elsevier, Amsterdam, 1986, pp. 239–257 (Chapter 8).
- [39] J.R. Bourne, B. Hamel, J.W. Ward, A discriminant-analysis-based scoring system for the electroencephalogram, in: *Conference Proceedings IEEE Southeastcon 80*, IEEE Press, New York, 1980.
- [40] J.R. Bourne, V. Jagannathan, B. Giese, J.W. Ward, A software system for syntactic analysis of the EEG, *Comp. Programs Biomed.* 11 (1980) 190–200.
- [41] V. Jagannathan, An artificial intelligence approach to computerized electroencephalogram analysis, Ph.D. Thesis, Vanderbilt University, Nashville, TN, 1981.
- [42] A.N. Mamelak, J.J. Quattrochi, J.A. Hobson, Automated staging of sleep in cats using neural networks, *Electroencephalogr. Clin. Neurophysiol.* 79 (1991) 52–61.
- [43] A.C. Tsoi, D.S.C. So, A. Sergejew, Classification of electroencephalogram using artificial neural networks, in: J.D. Cowan, G. Tesauero, J. Alspector (Eds.), *Proceedings of the sixth Conference on Advances in Neural Information Processing Systems (NIPS-93)*, 1993, pp. 1151–1158.
- [44] F.Y. Wu, J.D. Slater, L.S. Honig, R.E. Ramsay, A neural network design for event-related potential diagnosis, *Comp. Biol. Med.* 23 (1993) 251–264.
- [45] B. Klöppel, Neural networks as a new method for EEG analysis, *Pharmacoelectroencephalography* 29 (1994) 33–38.
- [46] Y. Si, J. Gotman, A. Pasupathy, D. Flanagan, B. Rosenblatt, R. Gottesman, An expert system for EEG monitoring in the pediatric intensive care unit, *Electroencephalogr. Clin. Neurophysiol.* 106 (1998) 488–500.
- [47] C.S. Herrmann, A fuzzy neural network for detecting graphoelements in EEGs, in: H.J. Herrmann, D.E. Wolf, E. Pöppel (Eds.), *Supercomputers in Brain Research: from Tomography to Neural Networks*, World Scientific, Singapore, 1995, pp. 193–198.
- [48] J. Gotman, Automatic detection of seizures and spikes, *J. Cog. Neurosci.* 16 (1999) 130–140.